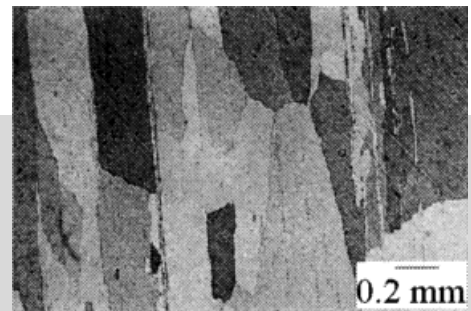


Manufacturing and Microstructural Evolution of Mechanically Alloyed Oxide Dispersion Strengthened Superalloys**

By Carlos Capdevila and Harry K. D. H. Bhadeshia*

Mechanical alloying is a process in which mixtures of powders are severely deformed until they form atomic solutions. Inert oxides can also be introduced to form a dispersion of fine particles which help strengthen the consolidated product. Significant quantities of iron and nickel-base alloys, with unusual properties, are produced commercially using this process. The total true strain during mechanical alloying can be as large as 9; there is proof that this leads to mixing on an atomic scale and to the development of a uniform grain structure which is sub-micrometer in size. Following mechanical alloying, the particles are consolidated using standard powder metallurgical techniques. The consolidated metal has a large stored energy, approaching 1 J g^{-1} . This ought to make it easy to induce recrystallisation, but in practice the alloys fail to recrystallise except at very high temperatures close to melting. On the other hand, the recrystallisation temperature can be reduced dramatically by slightly deforming the consolidated product prior to heat treatment. It is in this context that the solution formation, microstructure and mechanical properties of such alloys are reviewed here.



1. Introduction

An alloy can be created without melting, by violently deforming mixtures of different powders.^[1-4] Many modern oxide dispersion strengthened (ODS) iron and nickel base alloys are manufactured in this way, using high-energy milling to deform mixtures of elemental or alloyed metal powders. The effect of milling is to convert the heterogeneous mixture of powders into one in which each particle is a solid solution with an extremely fine grain structure. The inert oxides remain unmixed but are dispersed throughout the microstructure. They serve both to enhance the elevated temperature strength, and also the ambient temperature strength (even though this was not the primary reason for their insertion).

The mechanically-alloyed powder is usually hot compacted and extruded, or hot-rolled, to produce a fully dense material in the required shape (Fig. 1). There may be further

[*] Dr. C. Capdevila, Prof. H. K. D. H. Bhadeshia, FRS
University of Cambridge, Department of Materials Science
and Metallurgy
Pembroke Street, Cambridge CB2 3QZ (UK)

[**] We are grateful to the European Commission for funding the work via a BRITE-EURAM III project. It is a pleasure to acknowledge our project partners: Liverpool University, Plansee GmbH, Metall-Spezialrohr GmbH (MSR), Sydkraft, and Mitsui Babcock Technology Centre.

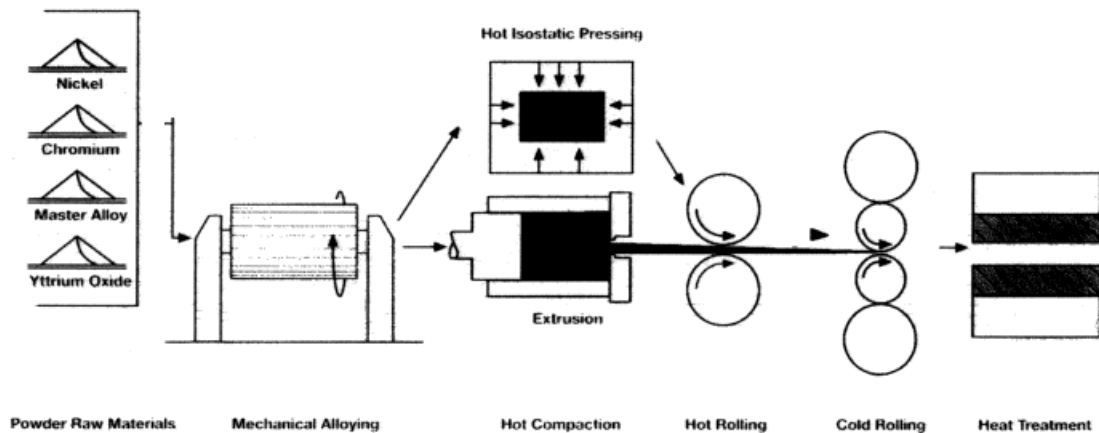


Fig. 1. Common method of manufacturing mechanically alloyed metals. The elemental powders/master-alloys/oxides are milled together to produce solid solutions containing dispersions of inert oxide particles. This powder is consolidated and the resulting material heat-treated to achieve a coarse, directional grain structure.

processing including heat-treatment to recrystallise the alloy, either into a coarse columnar grain structure suited to resist creep at high temperatures, or into fine equiaxed grains for ambient temperature applications. After final machining, the components may require assembly by mechanical means, for example using bolts or rivets, or by welding or brazing.

There are two main classes of alloys which are of commercial significance, the ODS iron-base superalloys and the ODS nickel-base superalloys. The chemical compositions of some of the commercial alloys produced using this method are listed in Table 1. They all contain chromium and/or aluminium for corrosion and oxidation resistance, and yttrium or titanium oxides for creep strength. Yttrium oxide cannot be

introduced into either iron or nickel by any method other than mechanical alloying; indeed, this was the motivation for the original work by Benjamin.^[1]

The alloys have wide-ranging applications, mostly in circumstances where a combination of creep strength and oxidation resistance is of paramount importance. For example, normal ferritic steels tend to undergo a marked loss in creep strength at temperatures in excess of 600 °C; the ODS alloys discussed here can in principle be used at much higher temperatures, perhaps as high as 1100 °C. The ferritic state makes them less susceptible to radiation-induced swelling. MA957 and DT2203Y05 are therefore designed for use in a liquid sodium environment at temperatures of the order of 700 °C.



Professor Harry Bhadeshia FRS is head of the Phase Transformations and Complex Properties Research Group at the University of Cambridge. He works on the theory of solid-state transformations with a view to attempting the design of metallic alloys, particularly those based on iron. He is the author or co-author of several textbooks and many research papers and review articles, the details of which can be found at <http://www.msm.cam.ac.uk/phase-trans>.



Dr. C. Capdevila works as a Research Associate in the Department of Materials Science and Metallurgy of the University of Cambridge. He deals mostly with phase changes which are thermodynamically of first order, i.e. they involve nucleation and growth with well-defined mechanisms of transformations and particular constraints to the achievement of equilibrium. More details of the work can be found at <http://www.msm.cam.ac.uk/phase-trans> and <http://www.cenim.csic.es>.

Table 1. Compositions (wt.-%) of some typical alloys. MA758 and PM1000 are nickel base mechanical alloys without γ' strengthening. The compositions of ODM061, DT, and DY are from Regle [56], as are the nitrogen data for MA956 and MA957.

Fe-base	C	Cr	Al	Mo	Ti	N	Ti ₂ O ₃	Y ₂ O ₃	Fe
MA957	0.01	14.0	–	0.3	1.0	0.012	–	0.27	Balance
DT2203Y05		13.0	–	1.5	2.2		–	0.5	Balance
ODM 331		13.0	3.0	1.5	0.6		–	0.5	Balance
ODM 751		16.5	4.5	1.5	0.6		–	0.5	Balance
ODM 061		20.0	6.0	1.5	0.6		–	0.5	Balance
MA956	0.01	20.0	4.5	–	0.5	0.045	–	0.50	Balance
PM2000	< 0.04	20.0	5.5		0.5		–	0.5	Balance
PM2010	< 0.04	20.0	5.5		0.5		–	1.0	Balance
DT		13.0	–	1.5	2.9		1.8	–	Balance
DY		13.0	–	1.5	2.2		0.9	0.5	Balance

Ni-Base	C	Cr	Al	Ti	W	Fe	N	Total O	Y ₂ O ₃	Ni
MA6000	0.06	15.0	4.5	2.3	3.9	1.5	0.2	0.57	1.1	Balance
MA760	0.06	19.5	6.0	–	3.4	1.2	0.3	0.6	1.0	Balance
MA758	0.05	30.0	0.3	–	0.5	–	–	0.37	0.6	Balance
PM1000		20.0	0.3	0.5		3.0			0.6	Balance

Both have a high void swelling resistance, and a low carbon concentration in order to avoid the formation of titanium carbides. The titanium is meant instead to combine with chromium, molybdenum, and iron to form a stable body-centred cubic FeCrTiMo intermetallic χ -phase during ageing at around 800 °C, which can further boost the creep strength. The rupture strength of ODM751 is larger than that of MA956.^[5] ODM751 has an additional 1.5 wt.-% Mo which, either via the χ -phase or through solid solution strengthening, is supposed to improve the creep strength. However, there are contradictory results; PM2000, which does not contain molybdenum, matches the rupture strength of ODM751.

Typical applications of PM2000 include use in furnace construction as shields or carrier systems; in the glass industry as stirrers or plungers in molten glass; in the combustion of waste materials; as thermocouple protection tubes; in high temperature testing-equipment; as burner tubes; a variety of applications in automotive diesel engines. Similarly, PM1000 is used in the manufacture of rotating discs for glass fibre production; for high temperature screws and fasteners; as face sheets in thermal protection panels; for space and aerospace engineering in general.^[6] MA956 sheet has been used in combustion chambers for turbines, for burner hardware in coal and oil burning power stations; MA974 for brazed nozzle guides in aero engines.^[4]

The nickel-base alloys MA6000 and MA760 are both γ' -strengthened, as in conventional nickel-base superalloys; the yttria allows the strength to be maintained to much higher temperatures.^[3] A lot of the oxidation resistance of MA6000 relies on the formation of chromia at the surface. However, chromia is not resistant to sulphidation, a factor important in industrial gas turbine manufacture, where the ODS alloys have applications as vanes. MA760 has higher chromium and aluminum concentrations, the latter inducing the formation of surface alumina.^[7]

2. Solution Formation During Mechanical Alloying

During mechanical alloying, the solution is prepared by mixing together solid-lumps of the components, each of which might contain many millions of identical atoms. Badmos and Bhadeshia^[8] examined the way in which an atomic solution ultimately evolves from these large lumps; it is relevant to ask the question: at what point in the size scale does the mixture of particles begin to exhibit solution-like behaviour? If there is no enthalpy of mixing, the problem reduces to one of finding the configurational entropy of mixtures of lumps as opposed to of atoms. A detailed thermodynamic analysis revealed that the entropy of mixing cannot be ignored when the particle sizes become less than a few hundreds of atoms.

In reality, there are no ideal solutions so the enthalpy of mixing will not be zero, but can be calculated using regular solution theory. However, the theory has to be adapted because unlike atomic solutions, the interacting atoms see each other only at the interfaces between particles. Only those atoms located at the interfaces participate in creating an enthalpy of mixing; this is, in effect, a chemical component of the interfacial energy. The structural component, for example via misfit dislocations, also makes a contribution which opposes mechanical alloying. This is because the interfacial area per unit volume increases with the inverse of the particle size. Therefore, it was predicted quantitatively by Badmos and Bhadeshia that atomic-solution formation is impossible since the cost of creating interfaces as the particles become ever smaller, overwhelms any tendency toward mixing! But experiments show that mixing does in fact happen. Badmos and Bhadeshia overcame this contradiction by proposing that there must be a gain in coherency as the particle size becomes smaller and smaller during mechanical alloying. The mechanism is illustrated in Figure 2 which shows how the structural component of interfacial energy decreases as the particle size decreases, via a gain in coherency. This is exactly the

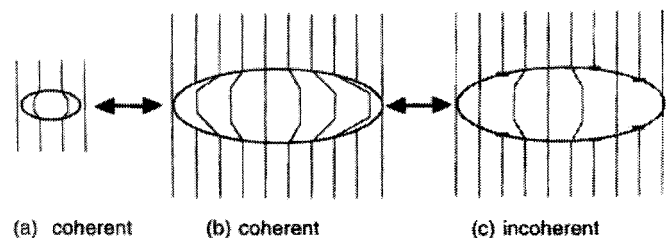


Fig. 2. The change in coherence as a function of particle size. The lines represent lattice planes which are continuous at the matrix/precipitate interface during coherence, but sometimes terminate in dislocations for the incoherent state. Precipitation occurs in the sequence a \rightarrow b whereas mechanical alloying is predicted to lead to a gain in coherence in the sequence c \rightarrow a.

opposite of what happens when a precipitate forms in the solid-state, starting as a coherent particle and losing coherency as it grows. Thus, solution formation is simply not possible without a gain in coherency during mechanical deformation; this is obvious in hindsight since we do not expect boundaries around individual atoms when an atomic solution forms in the solid-state.

The chemical component of interfacial energy becomes the regular solution enthalpy of mixing when an atomic solution has been achieved. This chemical component may oppose or favour solution formation when the enthalpy of mixing is positive or negative respectively. The structural component always opposes mixing unless the interfacial energy decreases as the particle size is reduced. On the other hand, the entropy of mixing always favours mixing. An interesting consequence of these conflicting tendencies is that there will be one or more barriers to solution formation, as illustrated in Figure 3; two barriers arise when the enthalpy of mixing is positive (the details are discussed in the literature^[8]).

3. Initial Microstructure

Immediately after the mechanical alloying process, the powders have a grain size which can be as fine as 1–2 nm locally.^[5] This is hardly surprising given the extent of the deformation during mechanical alloying, with true strains of the order of 9, equivalent to stretching a unit length by a factor of 8000. The consolidation process involves hot extrusion and rolling at temperatures of about 1000 °C, which causes recrystallisation into a sub-micrometer grain size (Fig. 4a). It is known that during the course of consolidation, the material may dynamically recrystallise several times.^[5,9–11] It should be emphasised that the sub-micrometer grains are not low-mis-

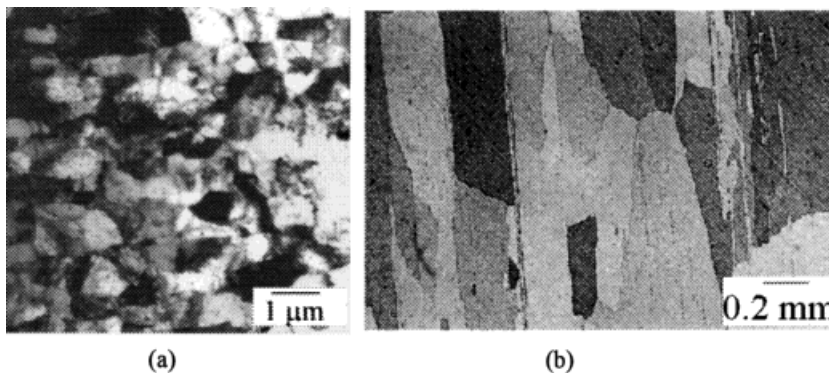


Fig. 4. a) Transmission electron micrograph showing the sub-micrometer grain structure of mechanically alloyed and consolidated iron-base MA957 alloy. The micrograph is a section normal to the extrusion direction. b) Optical micrograph showing the coarse, columnar recrystallisation grain structure resulting from heat treatment at 1400 °C.

orientation cell structures typical in aluminum alloys, but true grains with large misorientations.^[12] Subsequent heat-treatment leads to recrystallisation into a very coarse grained microstructure (Fig. 4b).

The extrusion and hot-rolling process leaves the microstructure of iron-base alloys in a cold-deformed state with elongated grains and a dislocation density of about 10^{15} m^{-2} .^[13] By contrast, the nickel-base alloys have fine, clean, equiaxed grains in a primary recrystallised state. The deformation processing causes an alignment of dispersoids along the working direction, particularly in the iron-base alloys^[12,14,15] (Fig. 5). This alignment reflects inhomogeneities in the fabrication process arising at the single particle level^[9] and below.

4. Recrystallisation

The alloys are very hard in the consolidated state (Table 2) and their fine grain structure is not appropriate for elevated temperature applications where resistance to creep is a prime requirement. They are therefore recrystallised to greatly coar-

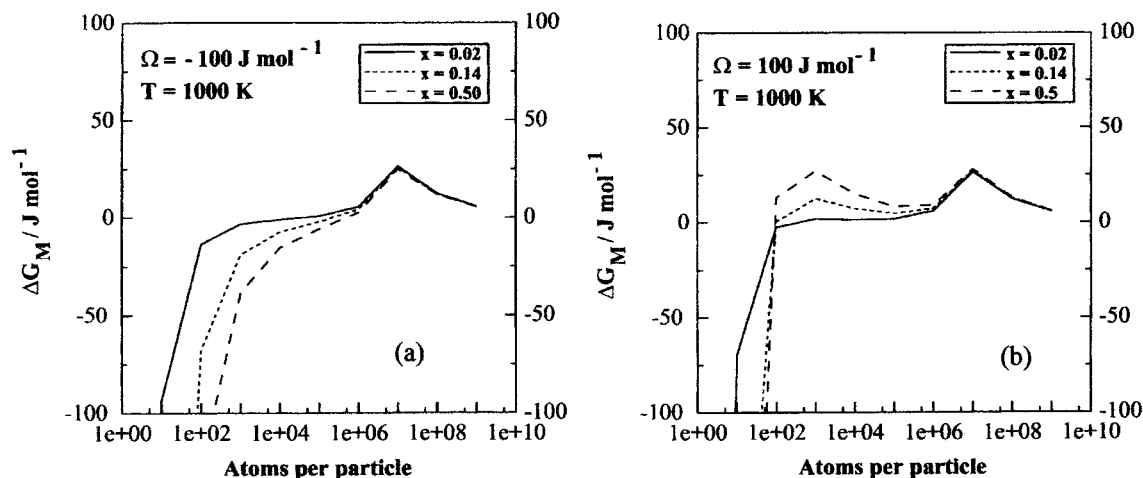


Fig. 3. Thermodynamic barriers to solution formation. a) Case where the enthalpy of mixing (Ω) is negative, i.e., unlike atoms attract. b) Case where there is a tendency to cluster with a positive enthalpy of mixing [8].

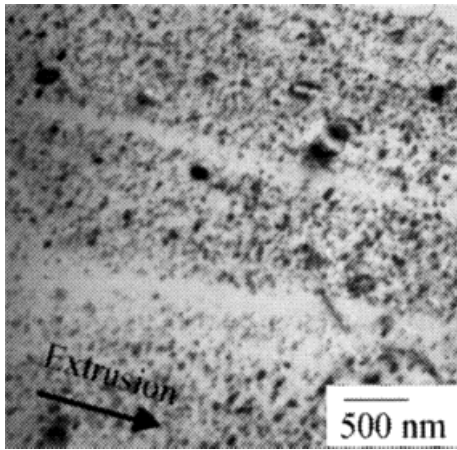


Fig. 5. Particles alignment along the extrusion direction of recrystallised PM2000 tube.

Table 2. Vicker's hardness data for commercial alloys, before and after recrystallisation.

Alloy	HV, before recrystallisation	HV, after recrystallisation
PM2000	400	290
MA957	400–410	230–240
MA956	350–390	225–245
MA956Sheet	410	250
PM1000	550	250
MA6000	645	500–520
MA760	720–790	500–515
MA758	405	214

sen the grains and to reduce the amount of grain surface per unit volume by some 2–3 orders of magnitude.

A remarkable feature of the alloys listed in Table 1 is that they can recrystallise into a columnar grain microstructure; these grains can be as long as the sample size and some hundreds of micrometers in width.^[1] The grains grow anisotropically because of the particle alignment discussed in the previous section. Hence, iron-base alloys develop columnar grains parallel to the extrusion direction irrespective of whether they are isothermally annealed, zone-annealed or cross-annealed (i.e., zone annealed along a direction normal to the extrusion direction). The distribution of particles is more isotropic in the nickel alloys; consequently, the direction of columnar grain growth can be controlled by the orientation of the temperature gradient during zone annealing. Indeed, equiaxed coarse grained secondary recrystallised microstructures can be readily generated in the nickel alloys, either by isothermal annealing or by zone annealing at high speeds.^[16]

Notice that the limiting grain size, obtained by balancing the particle pinning against the force driving grain boundary motion, is very large. Although particle pinning has a role in the development of anisotropic recrystallisation microstructures, it does not control the scale of the grains that grow. The scale seems to be determined by the nucleation process as discussed below.

4.1. Recrystallisation Temperature

The alloys recrystallise at exceptionally high homologous temperatures, some 0.9 of the absolute melting temperature (T_M). This contrasts with $0.6T_M$ in ordinary variants of similar metallic alloys. Strangely enough, the mechanically alloyed metals contain more stored energy than conventional metals which recrystallise at lower temperatures (Table 3). Notice that whereas the stored energy is large in the context of deformed metals, it is small when compared with other metastable materials such as amorphous metals or some solutions where solutes are trapped.

Several mechanisms have in the past been proposed to explain the high recrystallisation temperatures (T_R) in the range 1300–1450 °C. Early work on the nickel alloys^[17] tended to attribute the high T_R to the presence of γ' -precipitates. However, T_R is sometimes less than the temperature at which γ' dissolves and the iron-base alloys do not contain γ' and yet show exceptionally large values of T_R .

It has been speculated^[18,19] that solute-drag limits grain boundary mobility until a temperature is reached where the solute atmosphere evaporates. The idea is inconsistent with the observations that the recrystallisation temperature can be greatly reduced by a low-temperature heat treatment in the recovery range,^[18] or by other processing.^[20,21] In any event, solute-drag is a feature of all commercial alloys which are impure so it is hard to see why the mechanically alloyed ODS alloys should show exceptional behaviour. There is a claim that molybdenum segregates to grain boundaries in MA957,^[22] and that the low diffusivity of molybdenum inhibits grain boundary mobility. In fact, molybdenum diffuses faster in iron than iron itself.^[23] Miodownik et al.^[24] found excess titanium at a grain boundary in an extruded and heat treated bar of MA957 but the experiment should have been carried out on a partly recrystallised sample since it is segregation at the recrystallisation front which matters.

Other work^[25–27] has suggested that particles of yttrium oxide or various yttria/alumina compounds (spinel) must

Table 3. Enthalpy of recrystallisation [18,28,57,58]. The last two columns place the excess energy in context, with some data are from Turnbull [59]. T_M is the melting temperature and R the gas constant. For details see [12].

Alloy	Stored Energy [Jg^{-1}]	Materials Example	Stored Energy/ RT_M
MA957	≈ 1.0	Supersaturated Solution	<1
MA956	0.4	Intermetallic Compounds	<0.5
MA956sheet	≈ 0.4	Amorphous Solids	<0.5
MA6000	0.6	Compositionally Modulated Films	<0.1
MA760	1.0	Interphase Dispersions	<0.1
MA758	0.3	Commercial Mechanical Alloys	<0.005

coarsen before recrystallisation can occur. However, as pointed out earlier, the limiting grain size is in fact very large. Furthermore, T_R is found to be insensitive to changes in the particle pinning force.

It has been argued that a critical value of kinetic strength is required before the onset of recrystallisation.^[16] Kinetic strength is the product $t \exp\{-Q/RT\}$ for an isothermal heat treatment, where t is the heat treatment time and Q is an empirical activation energy. The concept is readily generalised for anisothermal processes by integrating over time and temperature. But there is no explanation in it for the particular kinetic strength needed, nor for the magnitude of Q which turns out to be some ten times greater than that for the self diffusion of the base element. More fundamental approaches using conventional nucleation and growth theory in combination with the Johnson–Mehl–Avrami method for overall transformation kinetics, also reveal a very large activation energy.^[28]

The difficulties are resolved as follows. The nucleation of recrystallisation in the present context begins by the bowing of a grain boundary. This normally is straightforward because the size of the boundary perturbation is small when compared with the grain size. However, with very small grains, the boundary junctions themselves act as severe pinning lines restricting bowing (Fig. 6). This leads to an enormous activation energy Q for the nucleation of recrystallisation, ten times larger than Q_D which is the activation energy for self diffusion.^[29,30] Q is reduced if a few grains happen to be larger; indeed, any non-uniformity introduced into the microstructure, for example by inhomogeneous deformation, will lead to a large decrease in T_R .^[15,21,31,32]

This model suggests that the individual grains cannot be considered to be topologically independent when the grain size becomes small. It explains the observed high values of T_R which are independent of alloy type; the common feature of

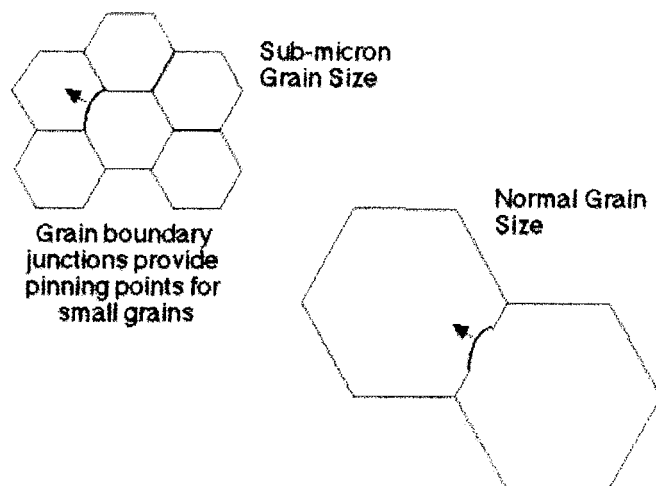


Fig. 6. Grain boundary bulging leading to the nucleation of recrystallisation can occur readily when the grain junctions are widely spaced, at distances greater than the critical bulge size. With sufficiently fine grains in the unrecrystallised microstructure, the grain junctions themselves are pinning points, making it very difficult to form recrystallisation nuclei.

the iron and nickel base alloys is the fine grain structure following the mechanical alloying process. It is predicted correctly that the recrystallisation temperature should decrease if the stored energy is reduced by a low-temperature heat treatment which leads to uniform grain coarsening. Since recrystallisation should eventually become more difficult as the stored energy is reduced, the curve of recrystallisation temperature versus grain size (or stored energy) should show a minimum. This too has been verified experimentally.^[30]

4.2. Cold Deformation

Regle and Alamo^[33] have conducted extensive studies on the recrystallisation behaviour of MA956 and MA957, for samples which were cold deformed after extrusion. Two deformation processes were used, swaging and drawing, with reductions ranging from 10 → 60 %.

Swaging and drawing led to quite different changes in crystallographic texture, and indeed to the subsequent recrystallisation behaviour. In all cases, deformation led to a reduction in the recrystallisation temperature, the change being largest for the cold-drawn samples. For MA957, the maximum reduction in the recrystallisation temperature was found to be about 200 °C from 1450 → 1250 °C. The corresponding maximum reduction for MA956 was for the cold drawn samples, where the recrystallisation temperature could be reduced from 1350 → 750 °C.

Chou^[34] has measured the stored energies in the samples studied by Regle and Alamo. Surprisingly, he found no increase in stored energy with deformation; indeed, it appears that the deformation leads to a reduction in stored energy (Table 4). There is no clear explanation of the results, but it is possible that the cold deformation modifies the crystallographic texture. It is conceivable that the texture change both leads to a reduction in the stored energy, and at the same time, a reduction in the recrystallisation temperature. The texture could, for example, lead to the clustering of adjacent grains into similar orientations. This would lead to an increase in the effective grain size, thereby making the nucleation of recrystallisation easier.

There are some other results presented by Capdevila and Bhadeshia^[35] which are consistent with this interpretation. A sample which was deformed by bending (and hence contained a controlled deformation gradient) was subjected to a

Table 4. Cold drawn MA957. Differential scanning calorimetry (DSC) measurements at 20 K min⁻¹ (after Chou, unpublished research).

MA957	Recrystallisation		Stored Energy [J g ⁻¹]
	Start [°C]	Finish [°C]	
0 % drawn	1370	1412	0.93
30 % drawn	1018	1093	0.78
40 % drawn	998	1056	0.70
50 % drawn	989	1041	0.69
60 % drawn	980	1027	0.65

recrystallisation heat treatment. It was vividly demonstrated that the anisotropic recrystallisation grain structure became refined with the extent of deformation (Fig. 7). Thus, deformation must enhance the nucleation rate of recrystallisation, perhaps by the texture mechanism discussed above.

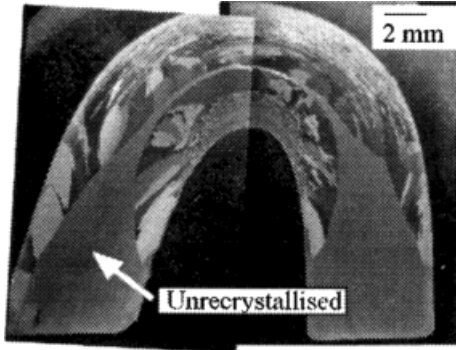


Fig. 7. Longitudinal section of bent sample recrystallised at T_R -30 °C (1300 °C) for 1 h.

4.3. Preannealing Effects

Preannealing describes heat treatment at a temperature which is below T_R , but high enough cause recovery with an accompanying reduction in stored energy.

Mild preannealing (≈ 1150 °C) has little or no effect on subsequent recrystallisation in MA957.^[18] An increase in the preannealing time causes a transition from a coarse columnar grain structure to one which is fine and equiaxed. The reduction in stored energy also reduces the grain boundary velocity, permitting nucleation in many locations thereby giving an equiaxed grain structure. Continued preannealing causes the development of a bimodal equiaxed grain structure. This is because there is an inhomogeneous distribution of pinning particles in the alloy. The now substantial reduction in stored energy retards recrystallisation more in some regions compared with others which are less strongly pinned. For MA957 the preannealing time at 1150 °C is in excess of 160 h for this condition to be reached. Further preannealing leads to such a large reduction in the stored energy that subsequent recrystallisation is completely suppressed.

It is much more difficult to similarly control the grain structure of MA956 using preannealing heat treatments. Grain refinement certainly occurs, as in MA957, but the fine grains tend not to be equiaxed. This may be because MA956 contains a larger concentration of yttria. The anisotropic pinning due to the inhomogeneous distribution of the oxide particles is more difficult to overcome if the fraction of particles is large. It would be very interesting to test this with MA956 containing a smaller quantity of yttria dispersoids. Finally, preannealing heat treatments do not affect the recrystallise grain structure in PM2000.

4.4. Crystallographic Texture

The major components of crystallographic texture in the mechanically alloyed steels are $\{001\} \langle 110 \rangle$, $\{111\} \langle \bar{1}10 \rangle$, which belong to the so-called α and γ fibres in crystal orientation distribution space.^[20,36] This applies both before and after recrystallisation; the latter simply changes the strength of the texture components relative to a random distribution of orientations. For reasons which are not obvious, recrystallisation seems easiest whenever the $\{111\} \langle \bar{1}10 \rangle$ is prominent (Table 5). Thus, MA956 prior to recrystallisation is rich in this particular component whereas MA957 is not, probably due to the presence of austenite in MA957 at the fabrication temperature.^[18] The former has a lower T_R compared with the latter, even though MA957 has a higher stored energy and lower yttria content than MA956. However, if MA957 is pre-annealed (i.e., heat-treated without recrystallisation) in order to make its texture comparable to that of MA956, then its recrystallisation temperature drops in spite of the reduction in stored energy due to the preannealing heat-treatment.

Evens et al.^[22] have also conducted microtextural measurements and interpreted their recrystallisation results in terms of the mobilities of grain boundaries with different orientations.

5. Assessment of Mechanical Properties

It is interesting to know, for example, the details of the origins of the strength of these alloys. Badmos and Bhadeshia^[37,38] analysed the mechanical properties of MA iron base ODS alloys as a function of the detailed chemical composition (Cr, Al, Ti, Mo, yttria), heat treatment, cold work, the test temperature, and the strain rate. An example of tensile strength calculations done using a neural network model is presented in (Fig. 8). They found that the ambient temperature yield strength of this alloy in the as-processed condition consists of contributions from its ultra-fine grain size, the intrinsic strength of ferritic iron, dispersoid strengthening via yttria compounds, and finally, the dislocation density, listed here in order of decreasing significance. The dispersoids contribute only ~ 250 MPa to the yield strength from a total of 1200 MPa, but their prime role of course is not to support the ambient temperature properties but rather, to provide creep resistance. Recrystallisation has the effect of virtually eliminating grain

Table 5. Crystallographic texture and recrystallisation [57].

	As-Received MA956	As-Received MA957	Preannealed MA957
Stored Energy [Jg^{-1}]	0.4	1.00	0.70
Recrystallisation Start	1273 °C	1429 °C	1362 °C
Recrystallisation Finish	1334 °C	1447 °C	1382 °C
Texture Summary	$\{111\} \langle \bar{1}10 \rangle$ $\{001\} \langle 110 \rangle$	Random	$\{111\} \langle \bar{1}10 \rangle$ $\{001\} \langle 110 \rangle$
Recrystallised Grains	Highly anisotropic	anisotropic	Equiaxed fine

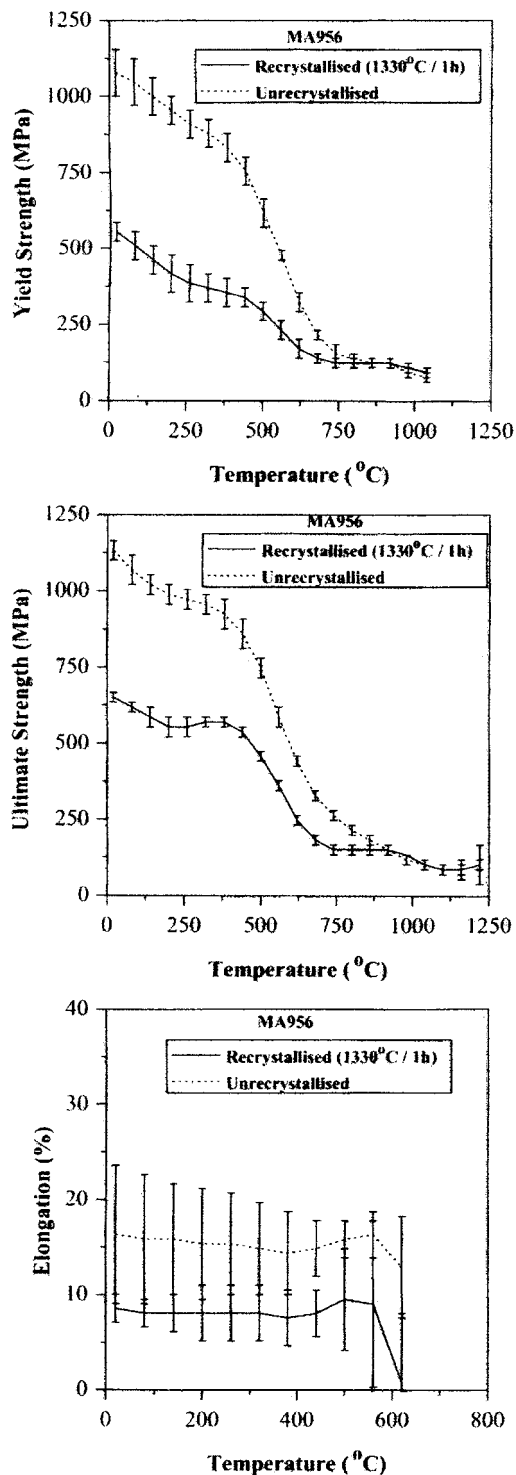


Fig. 8. Effect of temperature on yield strength, ultimate tensile strength, and percentage elongation of MA956.

size strengthening but leaving the other contributions essentially unchanged; the yttria dispersion is stable and does not remain essentially unaffected during recrystallisation.

The temperature dependence of the strength has also been estimated.^[39,40] The relatively sharp decline in the strength in the recrystallised condition beyond ~500°C replicates the decrease in the intrinsic strength of iron. Also, the greater

temperature dependence in the strength of the unrecrystallised specimen comes from dynamic recrystallisation during testing which reduces the grain size contribution to strength. Figure 9 shows the calculated yield strength and contributions from various components as a function of temperature for recrystallised MA956.

The methods used in the interpretation of the strength of MA alloys include a Bayesian estimate of uncertainty in the experimental data. This can be especially useful when assessing a large quantity of data in circumstances where the data are extremely noisy. Unfortunately, creep data for the iron-base MA alloys fall into this category. A way to illustrate that is to try to encrypt some of the published experimental data into a quantitative procedure for estimating the creep strain rate as a function of chemical composition (Cr, Al, Ti, Mo, yttria), temperature and applied stress. To deal with this goal, a database was compiled from the published literature, for of Fe-20Cr-5.5Al-0.5Y₂O₃ and Fe-13Cr-2.2Ti-1.5Mo-0.5Y₂O₃

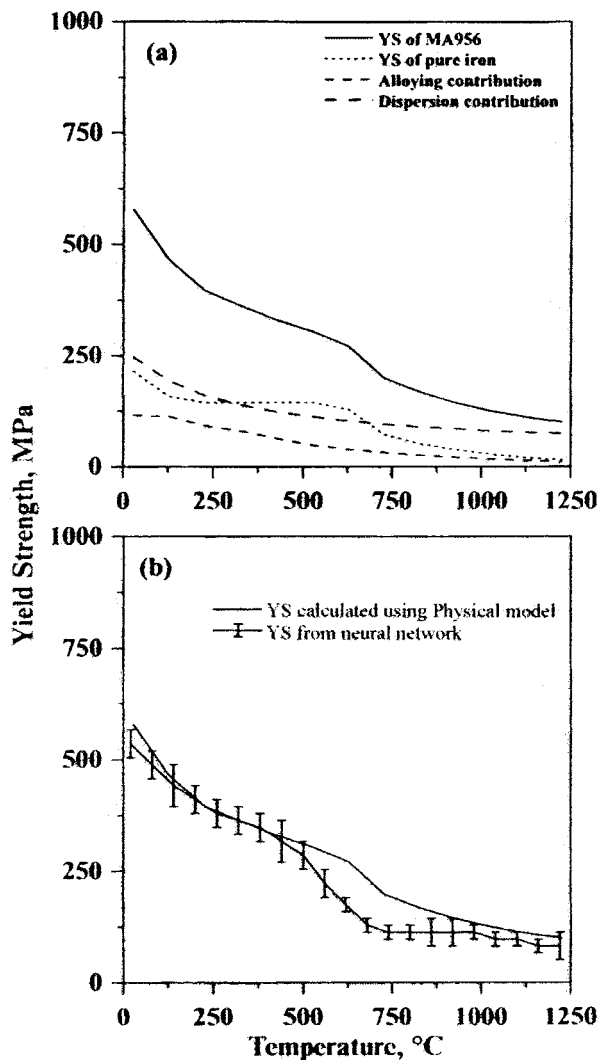


Fig. 9. a) Calculated yield strength (YS) of recrystallised MA956 and contributions from various components as function of temperature and b) calculated yield strength compared with results of neural network analysis.

alloys which are extensively reported in the literature.^[41–55] Figure 10 shows that the perceived level of noise (σ_v) in the creep strain rate is very large, and is not substantially reduced by making the model more complicated (N represents the number of hidden units in the neural network model, a reflection of the complexity of the model). Therefore, Figure 11 shows that there are great uncertainties in predicting the creep strain rate as a function of the variables that have been measured in the experiments. The methods shows vividly that the creep strain rate data are extremely noisy, indicating that there are many uncontrolled variables in the tests carried out to date.

6. Summary

Commercial mechanically alloyed, ODS materials have a fascination both in industry and in science. In industry they offer the possibility of metals which can serve under conditions normally reserved for the less reliable structural ceramics. In academia, they have revealed new phenomena about the recrystallisation process, apart from providing some of

the most beautiful grain structures visible to the naked eye. To paraphrase, a fine grain structure which is uniform, finds its incredibly difficult to recrystallise because the individual grains can no longer be considered to be topologically independent. Anything which introduces heterogeneity in such a microstructure will lead to a reduction in the recrystallisation temperature and a refinement of the grain structure due to increased nucleation.

There are a number of unanswered questions. An explanation is needed for the observed differences in the alignment of particles between iron and nickel alloys; measurements of the velocity of the recrystallisation front during isothermal heat treatment might reveal more about the mechanism by which coarse, columnar grain structures develop; what is the consequence of solute trapping, and the associated stored energy, on the recrystallisation behaviour and long term stability of the iron-base alloys?

Received: January 26, 2001

Final version: April 1, 2001

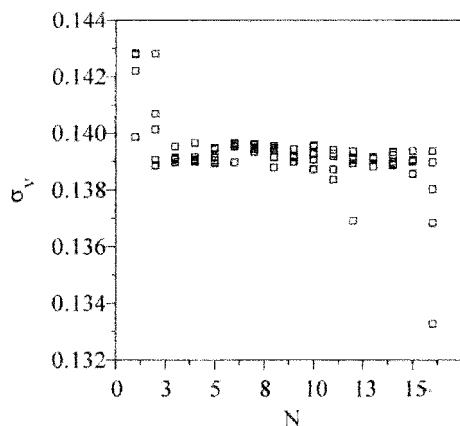


Fig. 10. Evolution of σ_v , which is the perceived level of noise in the creep data, as a function of N , which represents the number of hidden units in the neural network model, a reflection of the complexity of the model.

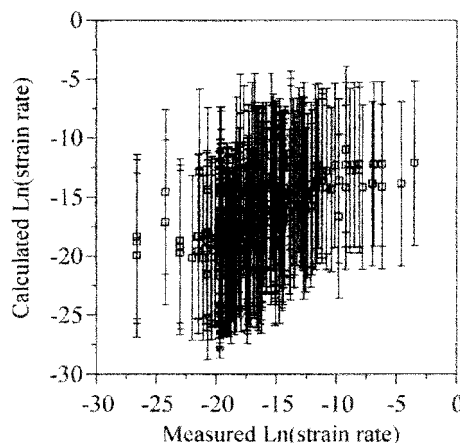


Fig. 11. Plot of estimated versus measured creep strain rate. The graph shows that there is a great deal of noise in the experimental data.

- [1] J. S. Benjamin, *Metall. Trans.* **1970**, *1*, 2943.
- [2] G. A. J. Hack, *Powder Metall.* **1984**, *27*, 73.
- [3] G. H. Gessinger, in *Powder Metallurgy of Superalloys*, Butterworths, London **1984**.
- [4] M. Baloch, H. K. D. H. Bhadeshia, *Mater. Sci. Technol.* **1991**, *6*, 1236.
- [5] D. M. Jaeger, A. R. Jones, in *Proc. of Materials for Combined Cycle Power Plant*, Institute of Metals, London **1991**, p. 1.
- [6] U. Miller, private communication, **2000**.
- [7] L. Patel, Private Communication, **1994**.
- [8] A. Y. Badmos, H. K. D. H. Bhadeshia, *Metal. Trans. A* **1997**, *28*, 2189.
- [9] D. M. Jaeger, A. R. Jones, in *Proc. of Processing, Properties and Applications of Metallic and Ceramic Materials* (Eds: M. H. Loretto, G. J. Beevers), Birmingham **1992**, p. 1.
- [10] D. M. Jaeger, A. R. Jones, in *Proc. of Materials for Advanced Power Engineering* (Ed: D. Coutouradis), Kluwer, Liege, Belgium **1994**, p. 1515.
- [11] D. M. Jaeger, A. R. Jones, in *Proc. of Materials for Advanced Power Engineering* (Ed: D. Coutouradis), Kluwer, Leige, Belgium **1994**, p. 1507.
- [12] H. K. D. H. Bhadeshia, *Mater. Sci. Eng. A* **1997**, *223*, 64.
- [13] E. A. Little, D. J. Mazey, W. Hanks, *Scripta Metall. Mater.* **1991**, *25*, 1115.
- [14] M. Baloch, *Ph.D. Thesis*, University of Cambridge **1989**.
- [15] C. Capdevila, Y. L. Chen, A. R. Jones, H. K. D. H. Bhadeshia, *Mater. Sci. Technol.*, **2001**, *17*, 693.
- [16] M. Baloch, H. K. D. H. Bhadeshia, *Mater. Sci. Technol.* **1991**, *6*, 1236.
- [17] Y. G. Nakagawa, H. Terashima, K. Mino, in *Proc. of Superalloys 1988* (Eds: S. Reichman, D. N. Duhl, G. Maurer, S. Antolovich, C. Lund), TMS, Warrendale, PA **1988**, p. 81.

- [18] T. S. Chou, H. K. D. H. Bhadeshia, *Mater. Sci. Technol.* **1993**, 9, 890.
- [19] P. Jongenburger, *Ph.D. Thesis no. 773*, Ecole Polytechnique Federale de Lausanne, Switzerland **1988**.
- [20] Alamo, H. Regle, J. L. Bechade, in *Advances in Powder Metallurgy and Particulate Materials—1992*, Metal Powder Industries Federation, Princeton, NJ **1992**, p. 169.
- [21] C. Capdevila, Y. L. Chen, A. R. Jones, H. K. D. H. Bhadeshia, in *Proc. of the 21st Riso International Symposium on Materials Science* (Eds: N. Hansen, X. Huang, D. Juul Jensen, E. M. Lauridsen, T. Leffers, W. Pantleon, T. J. Sabin, J. A. Wert), Riso National Laboratory, Denmark **2000**, p. 271.
- [22] P. J. Evens, J. W. Martin, E. A. Little, *Mater. Sci. Technol.* **1992**, 8, 531.
- [23] J. Fridberg, L. E. Torndahl, M. Hillert, *Jernkontorets Ann.* **1969**, 153, 263.
- [24] M. A. Miodownik, J. W. Martin, E. A. Little, *J. Mater. Sci. Lett.* **1993**, 12, 834.
- [25] A. P. Backhouse, S. S. Babu, K. Mino, H. K. D. H. Bhadeshia, *Pt. II Project Report*, Cambridge University, Cambridge **1991**.
- [26] M. Murakami, K. Mino, H. Harada, H. K. D. H. Bhadeshia, *Metall. Trans. A* **1993**, 24, 1049.
- [27] K. Murakami, *Ph.D. Thesis*, University of Cambridge **1993**.
- [28] W. Sha, H. K. D. H. Bhadeshia, *Metall. Trans. A* **1994**, 25, 705.
- [29] M. Murakami, H. Harada, H. K. D. H. Bhadeshia, in *Proc. of Heat Treatment '92* (Ed: I. Tamura), Kyoto, Japan **1992**, p. 269.
- [30] W. Sha, H. K. D. H. Bhadeshia, *Mater. Sci. Eng. A* **1997**, 223, 91.
- [31] C. Capdevila, H. K. D. H. Bhadeshia, Materials Algorithm Map, www.msm.cam.ac.uk/map/steel/programs/anrec.html.
- [32] C. Capdevila, H. K. D. H. Bhadeshia, Materials Algorithm MAP, www.msm.ca.ac.uk/map/steel/programs/tr_model.html.
- [33] H. Regle, A. Alamo, *J. Phys. IV* **1993**, 3-C7, 727.
- [34] T. S. Chou, *Ph.D. Thesis*, University of Cambridge **1994**.
- [35] C. Capdevila, Y. L. Chen, A. R. Jones, H. K. D. H. Bhadeshia, in *Proc. of the 21st Riso International Symposium on Materials Science* (Eds: N. Hansen, X. Huang, D. Juul Jensen, E. M. Lauridsen, T. Leffers, W. Pantleon, T. J. Sabin, J. A. Wert), Riso National Laboratory, Denmark **2000**, p. 277.
- [36] T. S. Chou, H. K. D. H. Bhadeshia, *Metall. Trans. A* **1993**, 24, 773.
- [37] A. Y. Badmos, H. K. D. H. Bhadeshia, *Mater. Sci. Technol.* **1998**, 14, 793.
- [38] A. Y. Badmos, H. K. D. H. Bhadeshia, *Mater. Sci. Technol.* **1998**, 14, 1221.
- [39] C. H. Young, H. K. D. H. Bhadeshia, *Mater. Sci. Technol.* **1983**, 10, 264.
- [40] W. C. Leslie, *Metall. Trans.* **1972**, 3, 5.
- [41] PLANSEE, *Internal report* **1998**, 1, 1.
- [42] M. Weise, F. Breutingger, J. Granacher, W. Blum, *Scr. Mater.* **1997**, 38, 1017.
- [43] H. D. Hedrich, in *Proc. of New Materials by Mechanical Alloying Techniques*, DGM Informationsgesellschaft, Stuttgart **1986**, p. 217.
- [44] S. Floreen, R. Kane, T. J. Kelly, M. L. Robinson, in *Proc. of Frontiers of High Temperature Materials*, Kluwer, Dordrecht, The Netherlands **1981**, p. 94.
- [45] B. Kazimierzak, M. Prignon, C. Lecomte-Mertens, D. Coutsouradis, in *Proc. of High Temperature Materials for Power Engineering 1990*, Kluwer, Dordrecht, The Netherlands **1990**, p. 131.
- [46] D. Sporer, O. Lang, in *Proc. of Materials for Advanced Power Engineering Part II*, Kluwer, Dordrecht, The Netherlands **1994**, p. 1471.
- [47] M. Rees, J. D. Parker, R. C. Hurst, in *Proc. of Materials for Advanced Power Engineering Part II*, Kluwer, Dordrecht, The Netherlands **1994**, p. 1573.
- [48] G. Korb, D. Sporer, *Proc. of High Temperature Materials for Power Engineering 1990*, Kluwer, Dordrecht, The Netherlands **1990**, p. 1417.
- [49] D. Sporer, K. Lempenauer, in *Proc. of the 13th International Seminar*, Plansee, Reutte **1993**, p. 796.
- [50] IncoMAP, *INCOLOY alloy MA956*, INCO, Hereford **1980**, p. 1.
- [51] J. D. Whittenberger, *Metall. Trans. A* **1981**, 12, 845.
- [52] R. Sundaresan, F. H. Froes, *J. Met.* **1987**, 8, 22.
- [53] R. W. Evans, J. A. Preston, B. Wilshire, *Mater. Sci. Eng. A* **1993**, 167, 65.
- [54] R. W. Evans, J. A. Preston, B. Wilshire, E. A. Little, *J. Nucl. Mater.* **1992**, 195, 24.
- [55] M. Weibe, W. Blum, in *Proc. of IX Conference on Electron Microscopy*, Krakow, Poland **1996**, p. 371.
- [56] H. Regle, *Ph.D. Thesis*, Universite de Paris-Sud **1994**.
- [57] T. S. Chou, H. K. D. H. Bhadeshia, *Mater. Sci. Eng. A* **1994**, 189, 229.
- [58] K. Murakami, K. Mino, H. Harada, H. K. D. H. Bhadeshia, *Metall. Trans. A* **1994**, 25, 652.
- [59] D. Turnbull, *Metall. Trans. A* **1981**, 12, 695.